Synthesis and characterization of Mn-doped ZnO nanorods grown in an ordered periodic honeycomb pattern using nanosphere lithography

S. Yılmaz [1,2 *], S. Garry [2], E. McGlynn [2], E. Bacaksız [3]

[1] Department of Material Engineering, Faculty of Engineering and Natural Sciences, Adana Science and Technology University, 01180 Adana, Turkey

[2] School of Physical Sciences and National Centre for Plasma Science and Technology, Dublin City University, Glasnevin, Dublin 9, Ireland

[3] Department of Physics, Faculty of Sciences, Karadeniz Technical University, 61080 Trabzon, Turkey

[*] Corresponding author: Tel: +90 322 455 00 00 Fax: +90 322 455 00 39
E-mail: slh_yilmaz@yahoo.com.tr (S. Yılmaz)

Abstract

We report a study of the structural, optical and magnetic properties of undoped and Mn-doped ZnO nanorods grown by chemical bath deposition in a periodic honeycomb lattice formation. Mn-doping is accomplished by a diffusion process at a constant time of 8 h for different temperatures of 500, 600 and 700 °C. Undoped and Mn-doped ZnO nanorods had a hexagonal wurtzite structure with a (002) preferred orientation. From SEM results, it was seen that Mn-doped ZnO nanorods grew vertically in the honeycomb lattice with lengths of 0.8 μm. XPS results showed that Mn^{3+} ions was successfully incorporated in the ZnO matrix by substituting for Zn^{2+} ions and that Mn-doping increased the number of oxygen vacancies in ZnO compared to undoped ZnO. This result was also supported by photoluminescence data at 10 K. Magnetic data showed that all the samples exhibited ferromagnetic character. Although the origin of undoped ZnO is related to oxygen vacancy-induced d^0 ferromagnetism, bound magnetic polarons are responsible from the ferromagnetism of Mn-doped ZnO samples which have T_c values above the room temperature.

Keywords: ZnO:Mn; nanorods; nanosphere lithography; oxygen vacancy; BMP

1. Introduction

In recent years, diluted magnetic semiconductors (DMS) have attracted significant interest due to their potential applications in spintronic devices. Among II-VI group semiconductors, especially, ZnO has gained lots of interest since it has a wide band gap of 3.37 eV with an excitonic binding energy of 60 meV at room temperature that make it an important material for potential optoelectronic applications [1]. ZnO is also a promising material in the investigation of DMS systems that can be achieved by doping with 3-d group elements like Mn, Co, Fe etc. and by these means the optical and magnetic properties of ZnO materials can be tuned. In particular, Mn-doped ZnO nanostructures have attracted significant interest as Mn has the highest magnetic moment and the first half of the d band is fully occupied [2]. The literature contains some reports of experimental studies on ZnO:Mn grown with diverse morphologies such as thin films, nanocrystals and nanowires and exhibiting room temperature ferromagnetism. For instance, Yang *et al.* produced Mn-doped ZnO thin films by the sol-gel technique on both glass and Si substrates and they found that even though undoped ZnO exhibited diamagnetic behavior, all the ZnO:Mn samples had a ferromagnetic character at room temperature. The origin of ferromagnetism was explained by the substitution of Mn^{2+} ions on Zn^{2+} sites [3]. Sain *et al.* synthesized ZnO:Mn nanocrystalline samples by mechanical alloying using a mixture of ZnO and MnO powders for different doping concentrations and room temperature ferromagnetism for ZnO:Mn samples was obtained. The origin of ferromagnetism was attributed to RKKY exchange interactions [4]. Furthermore, Philipose *et al.* grew ZnO:Mn nanowires by the vapor phase transport technique on Au-catalyzed Si substrates with Mn concentrations of 1, 2 and 4 at.%. They observed room temperature ferromagnetic character for 1 at.% Mn-doping and the ferromagnetism was attributed to the interactions between Mn ions and native defects [5].

ZnO material doped with transition-metal (TM) ions has been grown in various morphologies such as nanowires, nanorods and nanotubes [6-8]. Some methods to deposit TM-doped 1-D ZnO nanostructures include RF magnetron sputtering [9], vapor phase transport [10], pulsed laser deposition [11], spray pyrolysis [12] and chemical bath deposition (CBD) [13]. Among these methods, CBD is an attractive technique and offers advantages such as simple, low cost equipment and a low growth temperature [14]. To the best of our knowledge, this is the first study investigating the structural, optical and magnetic properties of Mn-doped ZnO nanorods grown into a periodic honeycomb pattern. Additionally, the study focuses on clarifying the origin of room temperature ferromagnetism observed in both

undoped and Mn-doped ZnO nanorods grown this honeycomb lattice using both photoluminescence and X-ray photoelectron spectroscopy results.

2. Experimental details

The experimental details concerning the growth of a ZnO buffer layer on Si substrates using both a seed layer followed by chemical bath deposition (CBD) can be found in [10]. To ensure spatially ordered nanostructure growth, ZnO buffer layer coated Si substrates were patterned using a modified nanosphere lithography (NSL) technique [15] whereby a close packed monolayer of polystyrene nanospheres (diameter 1 µm) are deposited on the sample. This nanosphere layer is then used as a template for a secondary silica mask [16]. Once deposited, the nanosphere layer is annealed at 110 °C for 40 s to ensure that each sphere has made good contact with the underlying ZnO buffer layer. Then a silica sol (prepared by mixing 1 ml of TEOS with 1 ml of 0.1 M HCl in 20 ml of absolute ethanol for three hours) is diluted 1:1 with absolute ethanol. 20 µl of this diluted sol is drop coated onto the annealed nanosphere layer. This is allowed to evaporate for a short period time before any excess is removed by spinning at 2500 rpm for 30 s. The silica is then left to dry in air before being heated to 90 °C for 10 mins. The nanospheres are then removed by dissolution in toluene, the substrate is rinsed in DI water and dried under a stream of nitrogen. Finally, the silica layer is densified by heating to 550 °C at a ramp rate of 15 °C min^{-1}. Using this method a periodic honeycomb silica lattice with periodic apertures exposing the underlying ZnO layer was formed. Vertically aligned ZnO nanorods were then deposited into the honeycomb pattern by the CBD process where 25 mM zinc acetate was dissolved in deionized water and the solution was heated at 70 °C and the substrates were submerged into the solution and kept at this temperature for two hours under stirring. After deposition, the samples were taken from the solution and cleaned with deionized water for five minutes. Finally, they were dried with nitrogen gas flow at room temperature. Introduction of Mn into ZnO nanorods was achieved by the evaporation of Mn metal using a thermal evaporation (Leybold Univex 350) system that had a pressure ~10^{-6} Torr during deposition. A thickness monitor (Inficon XTM/2) was used to control the evaporated Mn amount onto ZnO nanorods and thickness of the Mn layer was maintained at ~5 nm. After this process, the samples were annealed in a quartz tube at temperatures of 500 °C, 600 °C and 700 °C for 8 h in a vacuum of ~10^{-2} Torr.

X-ray diffraction (XRD) and X-ray rocking curve (XRC) studies were performed to investigate the crystal structure of the samples by means of a Bruker AXS D8 diffractometer with CuK_α radiation in the range of $2\theta = 20° – 60°$ with a step of 0.01°. Studies of surface

morphology and chemical composition were done with a Zeiss EVOLS 15 scanning electron microscope (SEM) which had an energy dispersive x-ray spectroscopy (EDS) attachment at an acceleration voltage of 20 kV. Detailed information about bonding at the surface was possessed via x-ray photoelectron spectroscopy (XPS) with Al K_α radiation (1486.6eV). The C 1s peak located at 285.0 eV was used as a reference for the charge-correction of binding energies of all the peaks. For the photoluminescence (PL) measurements at 10 K, a SPEX 1704 monochromator was employed with a closed cycle cryostat (Janis SHI-950-5) using an excitation 325 nm line of a He-Cd laser. Magnetization measurements of the specimens were conducted using a Quantum Design Physical Property Measurement System (PPMS) system.

3. Results and discussion

Fig. 1(a)-(d) show the XRD patterns of undoped and Mn-doped ZnO nanorods annealed at 500 °C, 600 °C and 700 °C for 8 h in vacuum, respectively. In all cases a dominant peak at 34.4° is seen, corresponding to the ZnO (002) reflection (JCPDS card no:36-1451), confirming the deposit as ZnO material with the normal hexagonal wurtzite structure. As seen from the figure, the strong (002) preferred orientation perpendicular to the substrate was observed for all the samples, indicating a highly textured deposit, following the seed layer texture [17,18], and this result is also supported by the SEM images discussed later. It is well-known that preferential orientation along the [002] crystallographic direction of ZnO is favorable in terms of thermodynamic aspects because deposition/growth on the (002) plane provides the lowest energy configuration on a variety of substrates [19]. A peak located at 56.3° was also observed for Mn-doped ZnO nanorods annealed at 700 °C for 8 h and was indexed as due to reflections from the (110) plane of ZnO, according to the JCPDS card referred to earlier. The appearance of this small peak at high annealing temperatures is probably due to slight misalignments in the seed and buffer layers at high temperatures as observed previously [18]. Neither MnO nor its binary compounds were seen in XRD studies of the samples, suggesting that Mn^{3+} substituted for Zn^{2+} in the ZnO host matrix without varying the wurtzite structure (confirmed by XPS results below). For the undoped ZnO sample, the *c* lattice parameter value of 5.20 Å was found from the (002) reflection peak centered at 34.45°. With respect to the undoped ZnO nanorods, no significant peak shift for the Mn-doped ZnO samples annealed at different temperatures for 8 h was seen.

The XRC results obtained from ZnO (002) diffraction peaks of undoped and Mn-doped ZnO nanorods (grown into the honeycomb pattern) annealed at 500 °C, 600 °C and 700 °C for 8 h in vacuum, respectively, are presented in Fig. 2. The undoped ZnO nanorods had a

full width at half-maximum (FWHM) value of 10.77°, confirming alignment perpendicular to the substrate surface. Upon Mn doping, the FWHM values decrease gradually with respect to undoped ZnO with increasing annealing temperature and reach a minimum value of 8.86° for Mn-doping at 700 °C, indicating a slightly improved alignment.

The top view SEM image of a monolayer of polystyrene nanospheres of 1μm diameter is shown in Fig. 3(a), implying that these nanospheres have a large and uniform coverage on the underlying ZnO buffer layer as well as the hexagonal close packing (hcp) structure. Fig. 3(b) shows the patterned silica honeycomb lattice on ZnO buffer layer coated Si substrates with apertures at the centre of each hexagon exposing the underlying ZnO layer. After well-aligned ZnO nanorods were grown into the honeycomb lattice, Mn evaporation and subsequent annealing was performed and SEM results are illustrated in Fig. 3 (c)-(f). Fig. 3(c) shows the plane view image of ZnO:Mn nanorods annealed at 700 °C for 8 h in vacuum which suggests that the pattern has a homogenous distribution of ZnO nanorods and each sphere was filled with a cluster of ZnO nanorods instead of one single nanorod. This result can be explained by the ZnO buffer layer providing multiple nucleation centers in the exposed region. A detailed study dealing with the effect of crystal quality was made by Szabo *et al.* for ZnO nanowires grown by a CBD technique on both polycrystalline sputtered ZnO thin film and ZnO single crystals [20]. Fig. 3(d)-(f) show the 45° tilted, 60° tilted and cross section images of ZnO:Mn nanorods annealed at 700 °C for 8 h, showing that these ZnO nanorods grew uniformly in a large area and perpendicular to the ZnO buffer layer coated Si substrate, consistent with the XRD and XRC results. The nanorod lengths were quite uniform at approximately 0.8 μm.

EDS measurements were made to determine the chemical composition of Mn element in the ZnO matrix. The EDS spectrum of ZnO:Mn nanorods annealed at 700 °C for 8 h is shown in Fig. 4 which confirms the presence of Zn, O, and Mn in the sample, as well as a Si signal due to the substrate. The atomic ratios of Mn/(Zn+O) for all the Mn-doped ZnO samples had almost constant values of ~ 0.5 at.% and their values did not significantly change with increase in the annealing temperature up to 700 °C.

XPS studies give useful information about the nature of Mn incorporation into the host matrix. Fig. 5(a) shows the survey spectrum of Mn-doped ZnO nanorods annealed at 500 °C for 8 h. From the figure, we see that Mn is present in the spectrum in addition to Zn, O and C. The core level peaks of the Mn elements (Mn $2p_{3/2}$ and Mn $2p_{1/2}$) are shown in Fig. 5(b) along with Gaussian peak fits. Mn $2p_{3/2}$ and Mn $2p_{1/2}$ peaks were located at the binding energy

values of 642.75 eV and 654.69 eV, respectively, meaning that Mn ions were successfully incorporated to the ZnO matrix as the valence state of +3. These results are in good agreement with reports in the literature [21, 22]. The O 1s peak data for undoped ZnO nanorods are presented in Fig. 5(c), indicating an asymmetric peak that is usually fitted with three components in the literature [23]. The binding energies of 530.39, 531.66 and 531.82 eV were obtained after fitting by Gaussian functions and are marked as O_L, O_M and O_H, respectively. The O_L peak is attributed to the lattice O^{2-} ions in the ZnO host matrix, the O_H peak is associated with the chemisorbed oxygen of the surface hydroxyl, CO_3, absorbed H_2O or absorbed O_2 [24]. On the other hand, the O_M peak is ascribed to oxygen deficient regions in ZnO, which imply the presence of oxygen vacancies (V_o) in the sample. The corresponding areas of the O_L, O_M and O_H peaks were labeled A_L, A_M and A_H, respectively. The ratio of $A_M/A_L+A_M+A_H$ was found to be ~0.46 for undoped ZnO samples whereas it increased to ~0.66 for Mn-doped ZnO nanorods annealed at 500 °C for 8 h shown in Fig. 5(d), meaning that Mn-doping and annealing enhanced the number of V_o defects.

Fig. 6(a)-(d) shows PL data measured at 10 K for undoped and Mn-doped ZnO nanorods annealed at 500, 600 and 700 °C for 8 h, respectively. Undoped ZnO nanorods exhibit a UV peak centered at 3.358 eV that is related to excitons bound to donors (D^0X). The intensity of this peak was fully quenched after Mn-doping together with vacuum annealing due to the strong nonradiative recombination processes and quenching associated with Mn atoms in ZnO [25]. Similar results were also reported by Inamdar and co-workers for Mn- and Co-doped ZnO nanocrystals [26]. In addition, the overall bandedge quenching trend for annealed samples is also consistent with that discussed by Wang and co-workers [27]. On the other hand, undoped ZnO also has a weak broad band betweeen 1.77 and 2.82 eV that is associated with deep level emission (DLE). This band is often associated with intrinsic defects such as Zn_i, V_{Zn}^-, V_o and O_i [28,29]. Upon Mn-doping and annealing at 500 and 600 °C for 8 h, two distinct bands located at ~500 nm and ~680 nm (2.48 eV and 1.82 eV, respectively) appear in the spectrum. The bands with energy values of 2.48 eV and 1.82 eV can be attributed to V_o and O_i defects, respectively, created in the sample due to the both vacuum annealing and Mn-doping treatment. With further increase of annealing temperature to 700 °C, it is noted that the relative peak intensity of the DLE reaches a maximum value, implying that the number of associated defects (especially V_o) significantly increased with respect to undoped ZnO, in good agreement with the XPS results discussed above.

M-H curves measured at 300 K for undoped and Mn-doped ZnO nanorods annealed at 500, 600 and 700 °C for 8 h, respectively are shown in Fig. 7(a)-(d). It is very clear from the

inset of Fig. 7 that the Si substrate has a diamagnetic behavior and its effect is subtracted from total magnetization of all the samples subsequently measured. As seen from Fig. 7, one surprising result is that undoped ZnO nanorods exhibited ferromagnetic character in addition to all the Mn-doped ZnO nanorod samples. The unexpected ferromagnetism in undoped ZnO nanorods may be ascribed to the defect-induced d^0 ferromagnetism, specifically related to the V_o defects observed in both XPS and PL data [30,31]. It is noted that the undoped ZnO nanorods had a saturation magnetization (M_s) of 0.004 emu/g. This value increased to 0.006 emu/g after Mn-doping with annealing at 500 °C for 8 h in vacuum. With further increase of annealing temperature to 600 °C, M_s reached a value of 0.01 emu/g. For the ZnO:Mn sample annealed at 700 °C for 8 h, M_s reached its maximum value of 0.02 emu/g. This gradual increase is an indication of the increased number of V_o defects in the ZnO:Mn samples with respect to undoped ZnO, consistent with both PL and XPS results. Based on all these results, we consider that the observed ferromagnetic character for all the ZnO:Mn nanorods is related to a bound magnetic polaron (BMP) model where there is an interaction among Mn^{2+} ions, the electronic carriers and V_o defects, first proposed by Coey *et al.* [32].

M-T data of Mn-doped ZnO nanorods annealed at 600 °C for 8 h is shown in Fig. 8. This measurement is performed at temperatures between 5 and 320 K at a magnetic field of 500 Oe. Above 120 K there is a significant decrease in magnetization value with increasing temperatures up to 320 K. It can be concluded from these data that our sample has a Curie temperature which is above room temperature. However, we cannot determine the exact Curie temperature of the sample owing our limited measurement range. In the literature, much lower T_c values (43 K and 60 K, respectively) were reported by Zheng *et al.* and Roy *et al.* in their studies of ZnO:Mn tetrapod [33,25].

4. Conclusions

In conclusion, the results of the study can be summarized as follows: (i) XRD data showed that all the samples had a (002) preferential orientation perpendicular to the substrate; (ii) SEM results indicated that undoped and Mn-doped ZnO nanorods were successfully grown in the periodic honeycomb pattern; (iii) the valence state of Mn ions in the ZnO was determined to be +3, indicating that Mn substitutes for Zn in the ZnO lattice, consistent with XRD data also; (iv) it was found from optical measurements that Mn-doping significantly enhanced the deep level emission of ZnO; (v) room temperature ferromagnetism was obtained for all the samples; (vi) the origin of ferromagnetism for undoped ZnO was attributed to V_o-

induced d^0 ferromagnetism, whereas a BMP model accounted for the origin of ferromagnetism in Mn-doped ZnO nanorods.

Acknowledgement: The first and corresponding author (SY) of the study would like to thank the Turkish Higher Education Council for its financial support to visit Dublin City University for an extended research stay. All the magnetic measurements reported in the study were carried out by Assoc. Prof. Dr. A. Ceylan and Prof. Dr. Ş. Özcan (Hacettepe University). All the authors are also grateful to Dr. M. Çopuroğlu and Prof. Dr. Ş. Süzer (Bilkent University) for XPS measurements.

References

[1] S.J. Pearton, C.R. Abernathy, M.E. Overberg, G.T. Thaler, A.F. Hebard, Y.D. Park, F. Ren, J. Kim, L.A. Boatner, Wide band gap ferromagnetic semiconductors and oxides, Journal of Applied Physics 93 (2003) 1-13.

[2] P. Sharma, A. Gupta, K.V. Rao, F.J. Owens, R. Sharma, R. Ahuja, J.M.O. Guillen, B. Johansson, G.A. Gehring, Ferromagnetism above room temperature in bulk and transparent thin films of Mn-doped ZnO, Nature Materials 2 (2003) 673-677.

[3] S. Yang, Y. Zhang, Structural, optical and magnetic properties of Mn-doped ZnO thin films prepared by sol–gel method, Journal of Magnetism and Magnetic Materials 334 (2013) 52-58.

[4] S. Sain, J. Bhattacharjeea, M. Mukherjee, D. Das, S.K. Pradhan, Microstructural, magnetic and optical characterizations of nanocrystalline $Zn_{1-x}Mn_xO$ dilute magnetic semiconductors synthesized by mechanical alloying**,** Journal of Alloys and Compounds 519 (2012) 112-122.

[5] U. Philipose, Selvakumar V. Nair, S. Trudel, C.F. de Souza, S. Aouba, Ross H. Hill, H.E. Ruda, High-temperature ferromagnetism in Mn-doped ZnO nanowires, Applied Physics Letters 88 (2006) 263101-263103.

[6] B. Pal, S. Dhara, P.K. Giri, Co-doped ZnO Nanowires Grown by Vapor-Liquid-Solid Methods: Structural, Optical and Magnetic Studies, Nano 7 (2012) 1250028-1250030.

[7] Z. Pan, P. Zhang, X. Tian, G. Cheng, Y. Xie, H. Zhang, X. Zeng, C. Xiao, G. Hu, Z. Wei, Properties of fluorine and tin co-doped ZnO thin films deposited by sol–gel method, Journal of Alloys and Compounds 576 (2013) 31-37.

[8] A. Fathalian, R. Moradiana, J. Jalilian, Half-metallic ferromagnetism in the Mn-doped zinc oxide nanotube, Solid State Communications 160 (2013) 17-21.

[9] C.G. Jin, T. Yu, Y. Yang, Z.F. Wu, L.J. Zhuge, X.M. Wu, Z.C. Feng, Ferromagnetic and photoluminescence properties of Cu-doped ZnO nanorods by radio frequency magnetron sputtering, Materials Chemistry and Physics 139 (2013) 506-510.

[10] S. Yılmaz, E. McGlynn, E. Bacaksız, Ş. Özcan, D. Byrne, M.O. Henry, R.K. Chellappan, Effects of Cu diffusion-doping on structural, optical, and magnetic properties of ZnO nanorod arrays grown by vapor phase transport method, Journal of Applied Physics 111 (2012) 013903-013909.

[11] W. Liang, B.D. Yuhas, P. Yang, Magnetotransport in Co-doped ZnO nanowires, Nano Letters 9 (2009) 892-896.

[12] S. Aksu, E. Bacaksiz, S. Yılmaz, I. Polat, M. Altunbaş, M. T. Türksoy, R. Topkaya, K. Özdoğan, Influence of the annealing atmosphere on structural, optical and magnetic properties

of Co-doped ZnO microrods, Physica E 44 (2012) 1244-1249.
[13] R.N. Gayen, A. Rajaram, R. Bhar, A.K. Pal, Ni-doped vertically aligned zinc oxide nanorods prepared by hybrid wet chemical route, Thin Solid Films 518 (2010) 1627-1636.
[14] S. Yılmaz, İ. Polat, Ş. Altındal, E. Bacaksız, Structural and electrical characterization of rectifying behavior in n-type/intrinsic ZnO-based homojunctions, Materials Science and Engineering B 177 (2012) 588-593.
[15] C. Li, G.S. Hong, P.W. Wang, D. P. Yu, L.M. Qi, Wet Chemical Approaches to Patterned Arrays of Well-Aligned ZnO Nanopillars Assisted by Monolayer Colloidal Crystals, Chemistry of Materials 21 (2009) 891-897.
[16] D. Byrne, E. McGlynn, J. Cullen, M.O. Henry, A catalyst-free and facile route to periodically ordered and c-axis aligned ZnO nanorod arrays on diverse substrates, Nanoscale 3 (2011) 1675-1682.
[17] L.E. Greene, M. Law, D.H. Tan, M. Montano, J. Goldberger, G. Somorjai, P.D. Yang, General Route to Vertical ZnO Nanowire Arrays Using Textured ZnO Seeds, Nano Letters 5 (2005) 1231-1236.
[18] D. Byrne, E. McGlynn, M. Biswas, M.O. Henry, K. Kumar, G. Hughes, A Study of Drop-Coated and Chemical Bath-Deposited Buffer Layers for Vapor Phase Deposition of Large Area, Aligned, Zinc Oxide Nanorod Arrays, Crystal Growth and Design 10 (2010) 2400-2408.
[19] M.H. Aslan, A.Y. Oral, E. Mensur, A. Gül, E. Basaran, Preparation of *c*-axis-oriented zinc-oxide thin films and the study of their microstructure and optical properties, Solar Energy Materials and Solar Cells **82** (2004) 543-552.
[20] Z. Szabo, J. Volk, E. Fülöp, A. Deak, I. Barsony, Regular ZnO nanopillar arrays by nanosphere photolithography, Photonics and Nanostructures: Fundamentals and Applications 11 (2013) 1-7.
[21] X. Yan, D. Hu, H. Li, L. Li, X. Chong, Y. Wang, Nanostructure and optical properties of M doped ZnO (M=Ni, Mn) thin films prepared by sol–gel process, Physica B 406 (2011) 3956-3962.
[22] R.K. Singhal, M.S. Dhawan, S.K. Gaur, S.N. Dolia, Sudhish Kumar, T. Shripathi, U.P. Deshpande, Y.T. Xing, Elisa Saitovitch, K.B. Garg, Room temperature ferromagnetism in Mn-doped dilute ZnO semiconductor: An electronic structure study using X-ray photoemission, Journal of Alloys and Compounds 477 (2009) 379-385.

[23] Z. Pan, P. Zhang, X. Tian, G. Cheng, Y. Xie, H. Zhang, X. Zeng, C. Xiao, G. Hu, Z. Wei, Properties of fluorine and tin co-doped ZnO thin films deposited by sol–gel method, Journal of Alloys and Compounds 576 (2013) 31–37.
[24] J.H. Li, D.Z. Shen, J.Y. Zhang, D.X. Zhao, B.S. Li, Y.M. Lu, Y.C. Liu, X.W. Fan, Magnetism origin of Mn-doped ZnO nanoclusters, Journal of Magnetism and Magnetic Materials 302 (2006) 118-121.
[25] V.A.L. Roy, A.B. Djurisic, H. Liu, X.X. Zhang, Y.H. Leung, M.H. Xie, J. Gao, H.F. Lui, C. Surya, Magnetic properties of Mn doped ZnO tetrapod structures, Applied Physics Letters 84 (2004) 756-758.
[26] D.Y. Inamdar, A.D. Lad, A.K. Pathak, I. Dubenko, N. Ali, S. Mahamuni, Ferromagnetism in ZnO Nanocrystals: Doping and Surface Chemistry, The Journal of Physical Chemistry C 114 (2010) 1451-1459.
[27] L Wang, Y. Pu, W. Fang, J. Dai, C. Zheng, C. Mo, C. Xiong, F. Jiang, Effect of high-temperature annealing on the structural and optical properties of ZnO films, Thin Solid Films 491 (2005) 323-327.
[28] H. Liu, X. Zhang, L. Li, Y.X. Wang, K.H. Gao, Z.Q. Li, R.K. Zheng, S.P. Ringer, B. Zhang, X.X. Zhang, Role of point defects in room-temperature ferromagnetism of Cr-doped ZnO, Applied Physics Letters 91 (2007) 072511-072513.
[29] X. Zhang, W.H. Wang, L.Y. Li, Y.H. Cheng, X.G. Luo, H. Liu, Z.Q. Li, R.K. Zheng, S.P. Ringer, Influence of oxygen partial pressure on the ferromagnetic properties of polycrystalline Cr-doped ZnO films, Europhysics Letters 84 (2008) 27005-27009.
[30] G. Xing, D.Wang, J. Yi, L. Yang, M. Gao, M. He, J. Yang, J. Ding, T.C. Sum, T. Wu, Correlated d_0 ferromagnetism and photoluminescence in undoped ZnO nanowires, Applied Physics Letters 96 (2010) 112511-112513.
[31] D. Gao, J. Zhang, G. Yang, J. Zhang, Z. Shi, J. Qi, Z. Zhang, D. Xue, Ferromagnetism in ZnO Nanoparticles Induced by Doping of a Nonmagnetic Element: Al, The Journal of Physical Chemistry C 114 (2010) 13477-13481.
[32] J.M.D. Coey, M. Venkatesan, C.B. Fitzgerald, Donor impurity band exchange in dilute ferromagnetic oxides, Nature Materials 4 (2005) 173-179.
[33] R.K. Zheng, H. Liu, X.X. Zhang, V.A.L. Roy, A.B. Djurisic, Exchange bias and the origin of magnetism in Mn-doped ZnO tetrapods, Applied Physics Letters 85 (2004) 2589-2591.

Figure Captions

Fig. 1. XRD patterns of undoped ZnO (a) and Mn-doped ZnO nanorods (grown into the honeycomb lattice) annealed at 500 °C (b), 600 °C (c), 700 °C (d) for 8 h.

Fig. 2. XRC results of undoped ZnO (a) and Mn-doped ZnO nanorods annealed at 500 °C (b), 600 °C (c), 700 °C (d) for 8 h.

Fig. 3. (a) A SEM image of monolayer of polystyrene nanospheres, (b) the honeycomb silica lattice atop the ZnO buffer layer coated Si substrates, (c) top view, (d) 45° tilted view, (e) 60° tilted view and (f) cross-section SEM images of Mn-doped ZnO nanorods (grown into the honeycomb lattice) annealed at 700 °C for 8 h.

Fig. 4. EDS spectrum of Mn-doped ZnO nanorods annealed at 700 °C for 8 h.

Fig. 5. (a) XPS survey spectra of Mn-doped ZnO nanorods annealed at 500 °C for 8 h, (b) indicates the core-level peak of Mn 2p and its Gaussian fitting, (c) and (d) show the core level peaks of O 1s together with Gaussian fitting for undoped ZnO and Mn-doped ZnO nanorods annealed at 500 °C for 8 h, respectively.

Fig. 6. Photoluminescence spectra (at 10 K) of undoped ZnO (a) and Mn-doped ZnO nanorods annealed at 500 °C (b), 600 °C (c), 700 °C (d) for 8 h.

Fig. 7. M-H loops at 300 K for undoped ZnO (a), Mn-doped ZnO nanorods annealed at 500 °C (b), 600 °C (c), 700 °C (d) for 8 h. M-H curve of bare Si substrate is presented in the inset.

Fig. 8. M-T curve of Mn-doped ZnO nanorods annealed at 600 °C for 8 h.

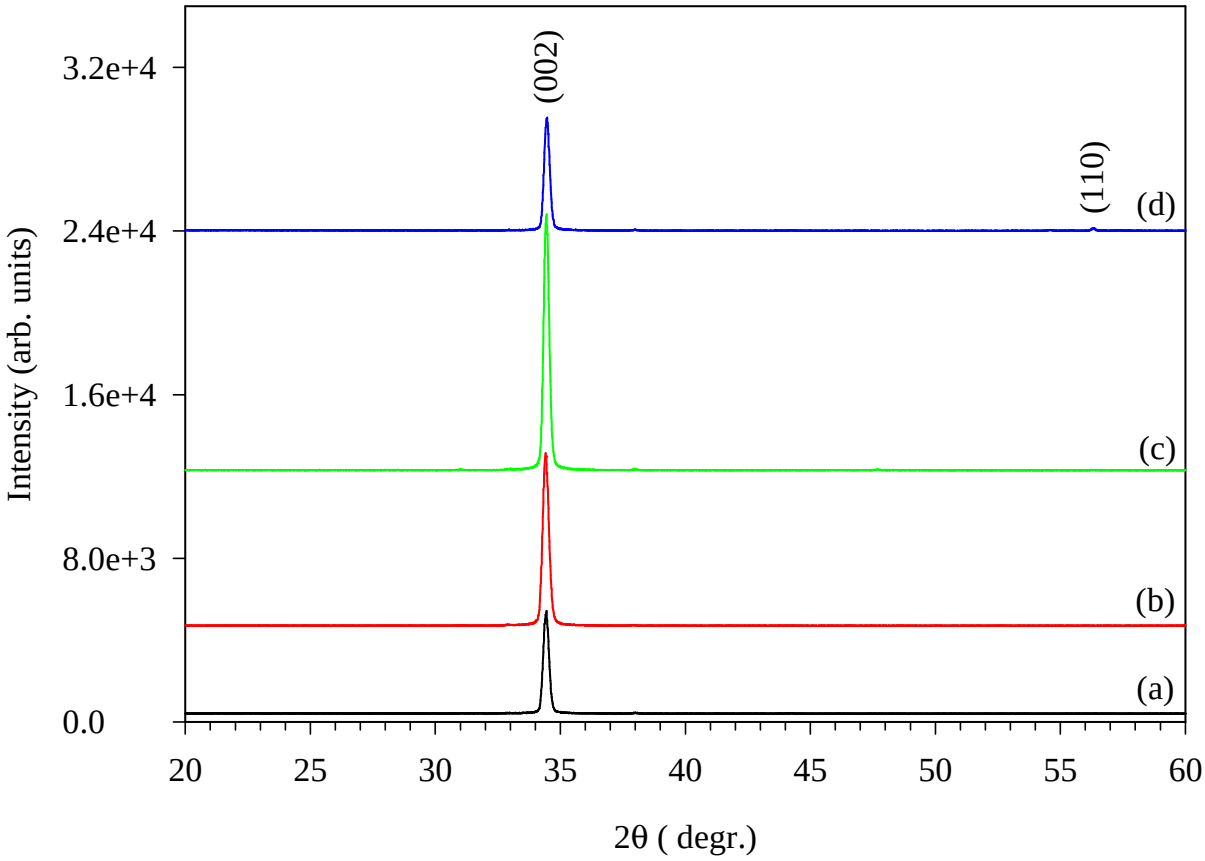
3.2e+4
2.4e+4
1.6e+4
8.0e+3
0.0
Intensity (arb. units)
(002)
(110)
(d)
(c)
(b)
(a)
20
25
30
35
40
45
50
55
60
2θ (degr.)

Fig. 1

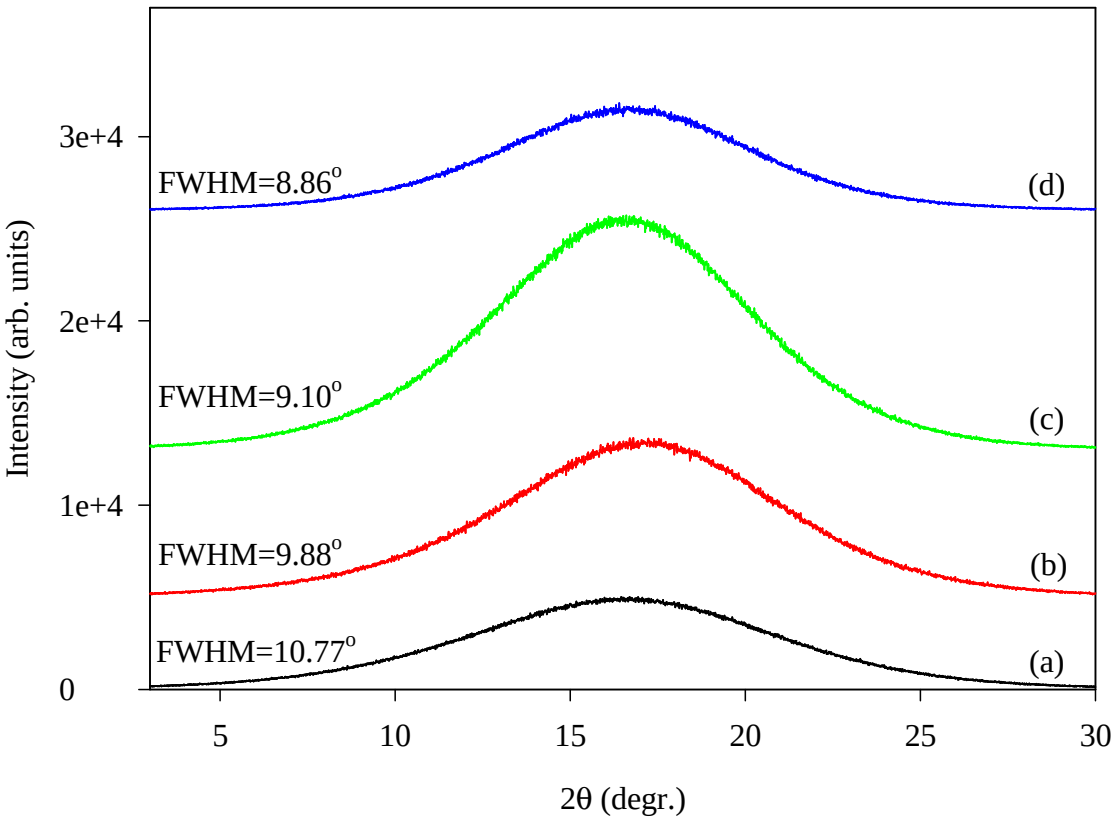
Intensity (arb. units)
3e+4
2e+4
1e+4
0
FWHM=8.86°
(d)
FWHM=9.10°
(c)
FWHM=9.88°
(b)
FWHM=10.77°
(a)
5
10
15
20
25
30
2θ (degr.)

Fig. 2

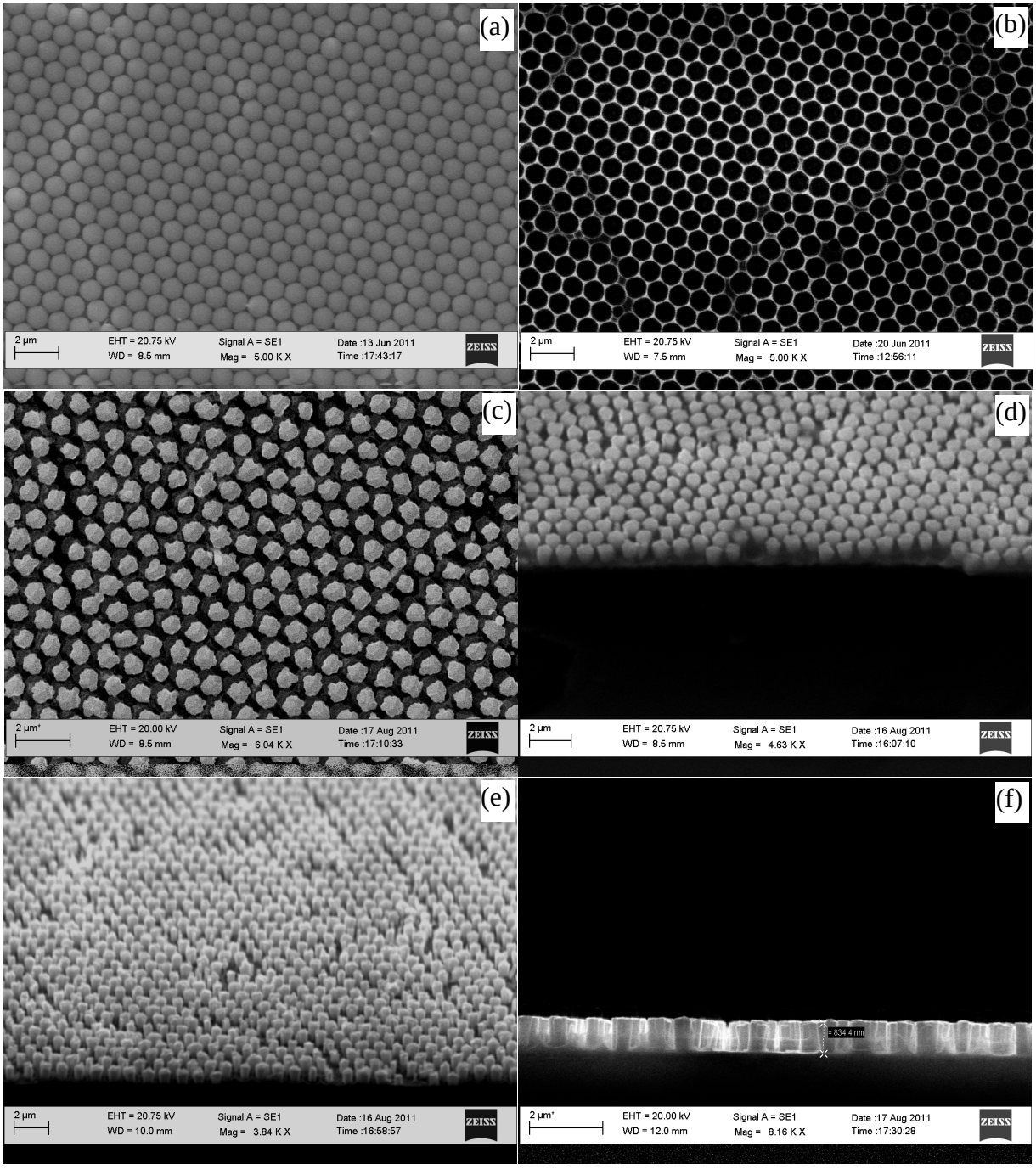
(a)
2 µm
EHT = 20.75 kV
WD = 8.5 mm
Signal A = SE1
Mag = 5.00 K X
Date :13 Jun 2011
Time :17:43:17
ZEISS
(b)
2 µm
EHT = 20.75 kV
WD = 7.5 mm
Signal A = SE1
Mag = 5.00 K X
Date :20 Jun 2011
Time :12:56:11
ZEISS
(c)
2 µm
EHT = 20.00 kV
WD = 8.5 mm
Signal A = SE1
Mag = 6.04 K X
Date :17 Aug 2011
Time :17:10:33
ZEISS
(d)
2 µm
EHT = 20.75 kV
WD = 8.5 mm
Signal A = SE1
Mag = 4.63 K X
Date :16 Aug 2011
Time :16:07:10
ZEISS
(e)
2 µm
EHT = 20.75 kV
WD = 10.0 mm
Signal A = SE1
Mag = 3.84 K X
Date :16 Aug 2011
Time :16:58:57
ZEISS
(f)
= 834.4 nm
2 µm
EHT = 20.00 kV
WD = 12.0 mm
Signal A = SE1
Mag = 8.16 K X
Date :17 Aug 2011
Time :17:30:28
ZEISS

Fig. 3

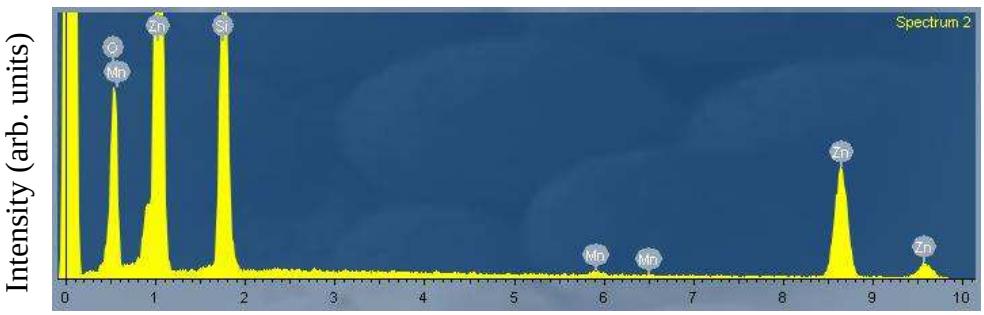
Intensity (arb. units)
Spectrum 2
O
Mn
Zn
Si
Mn
Mn
Zn
Zn
0
1
2
3
4
5
6
7
8
9
10
Energy (keV)

Fig. 4

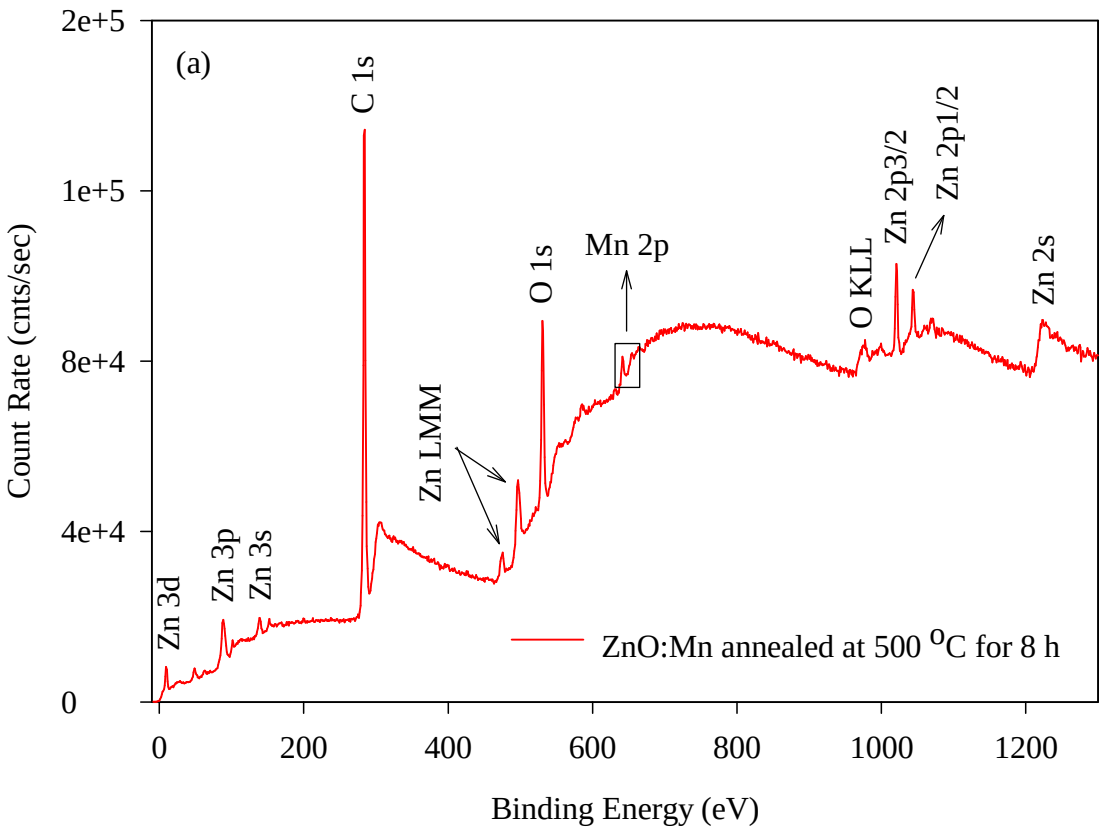
(a)
C 1s
Zn 2p1/2
Zn 2p3/2
O KLL
Mn 2p
O 1s
Zn LMM
Zn 2s
Zn 3p
Zn 3s
Zn 3d
ZnO:Mn annealed at 500 °C for 8 h
Count Rate (cnts/sec)
Binding Energy (eV)
2e+5
1e+5
8e+4
4e+4
0
0
200
400
600
800
1000
1200

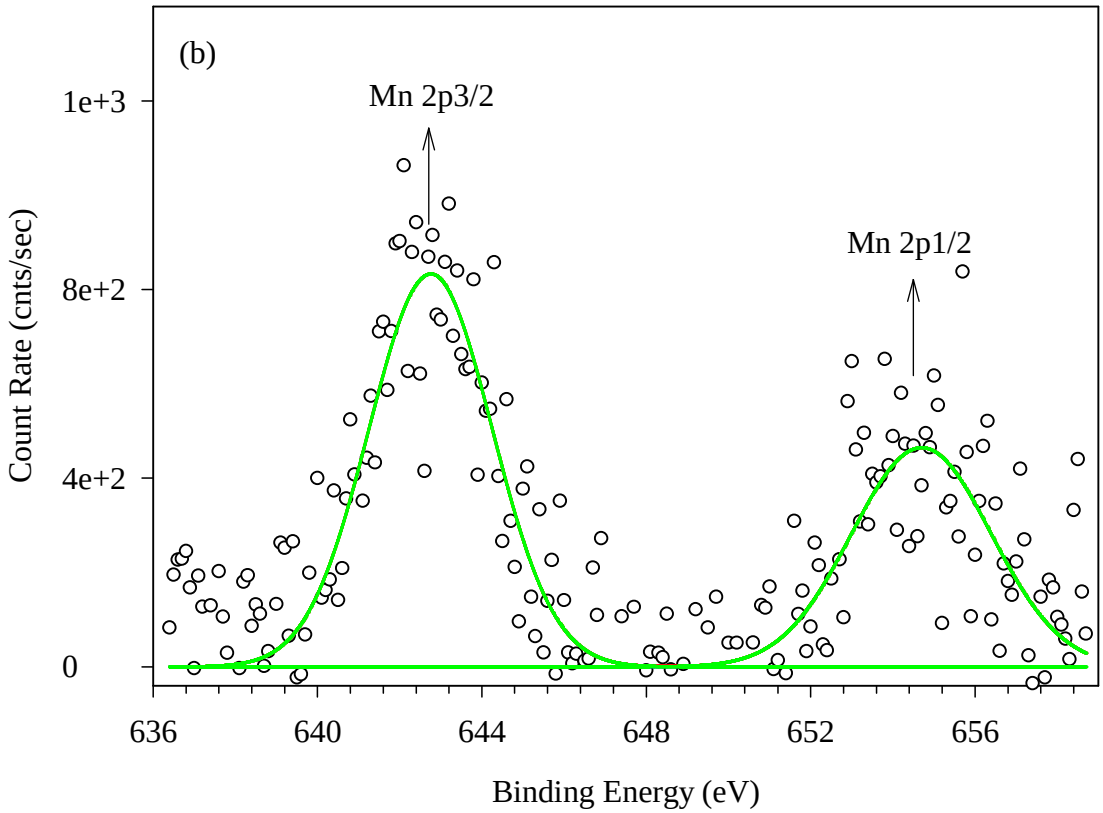
(b)
Mn 2p3/2
Mn 2p1/2
Count Rate (cnts/sec)
Binding Energy (eV)
1e+3
8e+2
4e+2
0
636
640
644
648
652
656

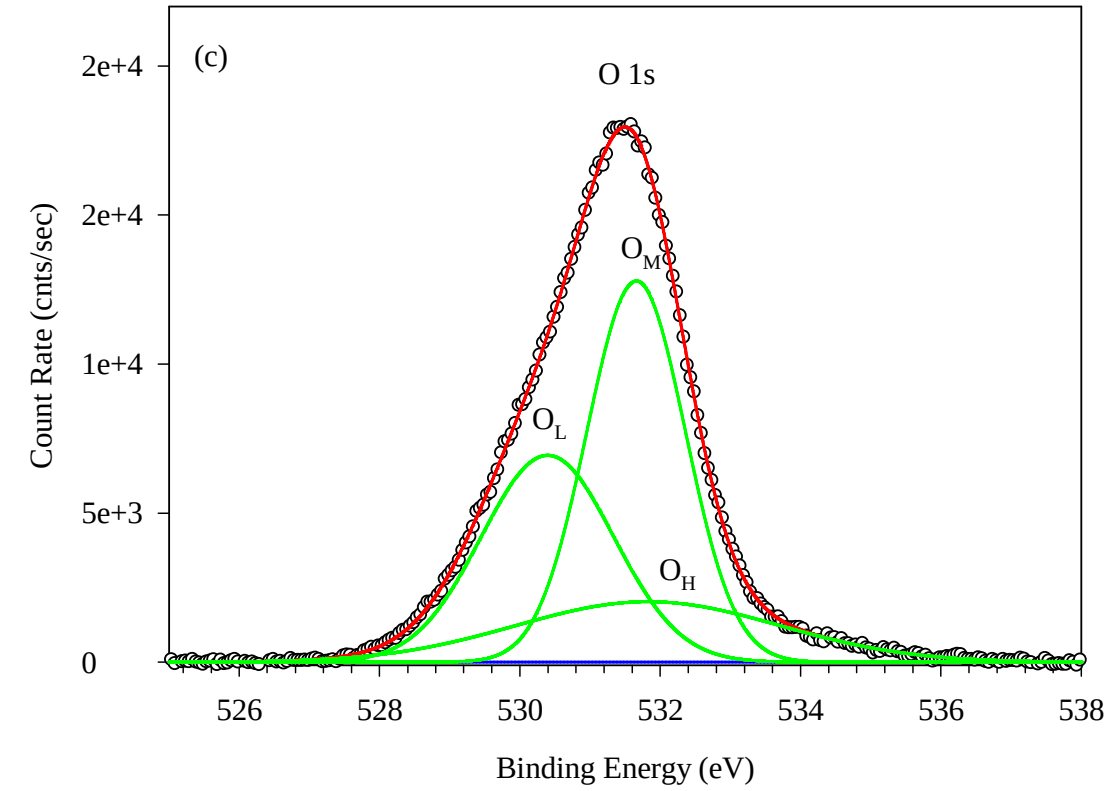
(c)
O 1s
O_M
O_L
O_H
Count Rate (cnts/sec)
2e+4
2e+4
1e+4
5e+3
0
526
528
530
532
534
536
538
Binding Energy (eV)

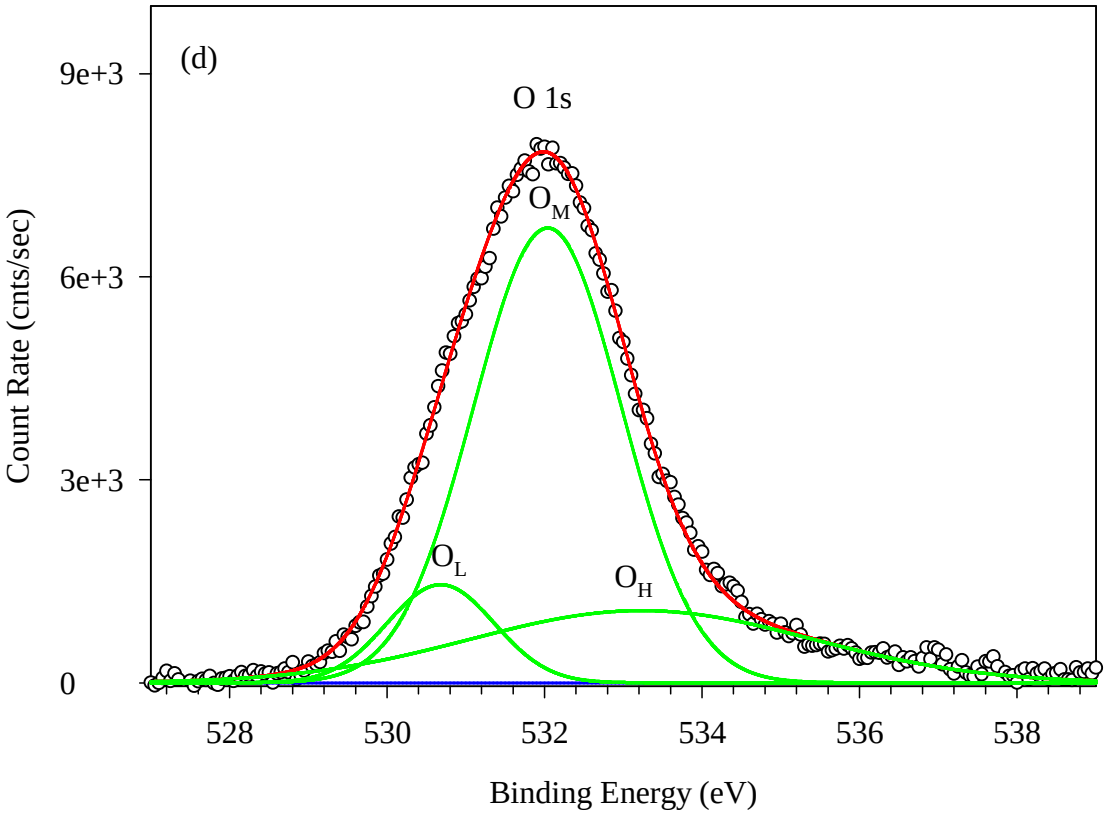
(d)
O 1s
O_M
O_L
O_H
Count Rate (cnts/sec)
9e+3
6e+3
3e+3
0
528
530
532
534
536
538
Binding Energy (eV)

Fig. 5

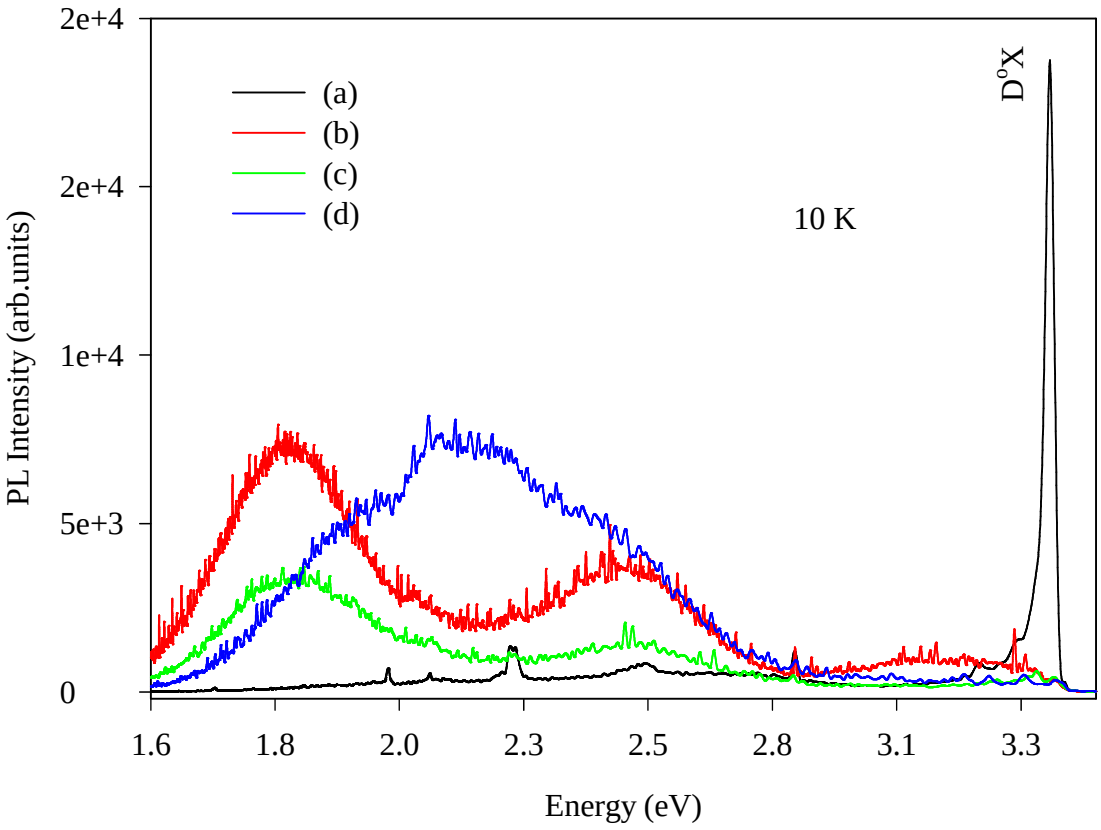
2e+4
2e+4
1e+4
5e+3
0
PL Intensity (arb.units)
(a)
(b)
(c)
(d)
10 K
D°X
1.6
1.8
2.0
2.3
2.5
2.8
3.1
3.3
Energy (eV)

Fig. 6

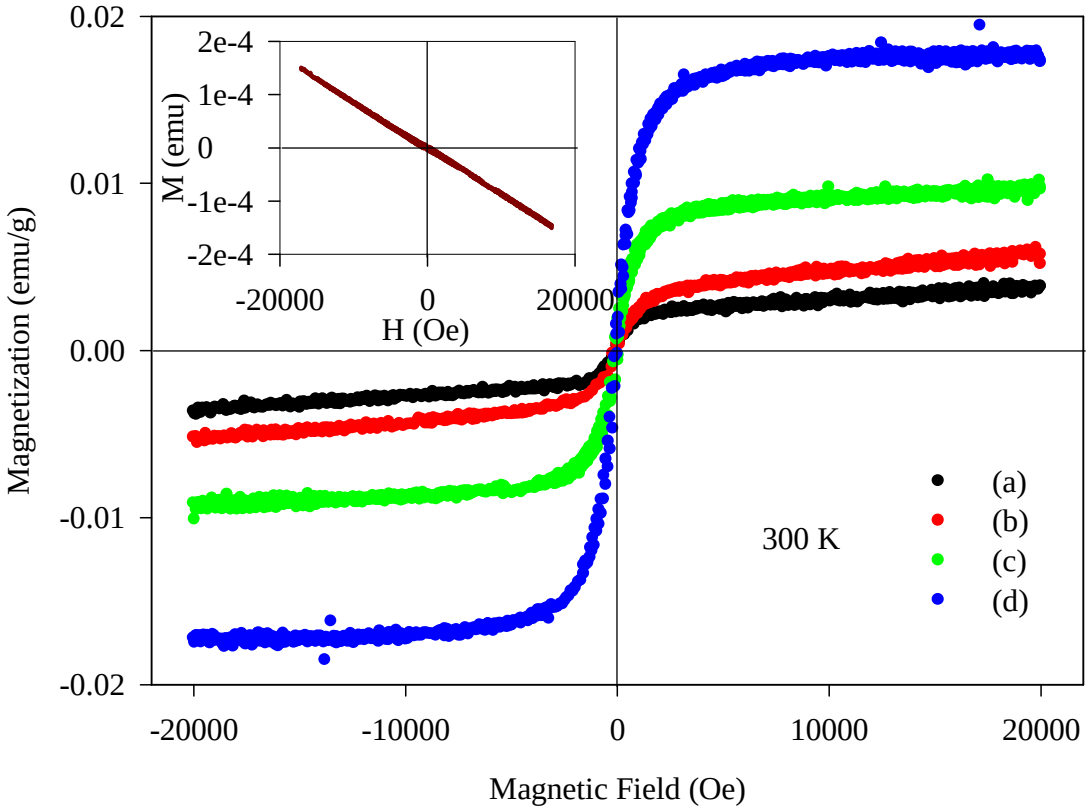
0.02
0.01
0.00
-0.01
-0.02
Magnetization (emu/g)
-20000
-10000
0
10000
20000
Magnetic Field (Oe)
2e-4
1e-4
0
-1e-4
-2e-4
M (emu)
-20000
0
20000
H (Oe)
300 K
(a)
(b)
(c)
(d)

Fig. 7

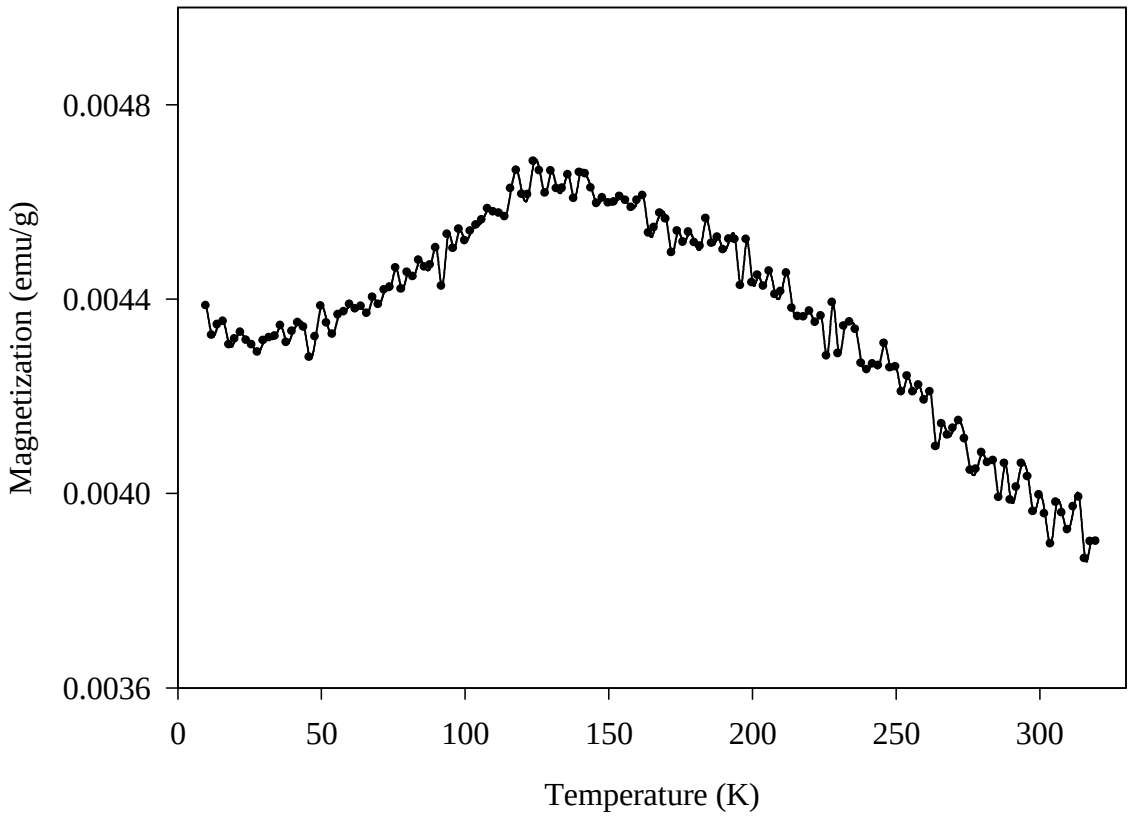
0.0048
0.0044
0.0040
0.0036
Magnetization (emu/g)
0
50
100
150
200
250
300
Temperature (K)

Fig. 8